RSC Advances

PAPER

View Article Online
View Journal | View Issue

Cite this: *RSC Adv.*, 2017, 7, 52947

Efficient interface and bulk passivation of PbS quantum dot infrared photodetectors by PbI_2 incorporation†

Keke Qiao,[a] Yulin Cao,*[b] Xiaokun Yang,[a] Jahangeer Khan,[a] Hui Deng,[a] Jian Zhang,[a] Umar Farooq,[a] Shengjie Yuan[a] and Haisheng Song *[a]

Received 20th September 2017
Accepted 26th October 2017

DOI: 10.1039/c7ra10422g

rsc.li/rsc-advances

Lead sulfide colloidal quantum dots (PbS CQDs) exhibit outstanding optoelectronic properties owing to their low temperature solution-processability and bandgap tunability. PbS QD heterojunction detectors suffer from an incomplete interface and bulk passivation. Herein, a simple passivation method based on PbI_2 was developed, which can effectively suppress the heterojunction interface and PbS QD surface defects by interface and ligand passivation. Utilizing the present strategies, PbS QD photodetectors can decrease the dark current and simultaneously increase the photocurrent. Such photodiode detectors also showed a fast response on the order of microseconds which is much faster than that of photoconductive CQD detectors (millisecond order). Also, an ultra-high specific detectivity of 10^{13} Jones was obtained. Meanwhile, the energy conversion efficiency of PbI_2 based devices reached 8%, a twofold value compared to the control one. The convenient and efficient passivation method is expected to hold great potential for high performance QD optoelectronic devices.

Introduction

Colloidal quantum dots (CQDs) are unique optoelectronic materials and have achieved rapid progress in various research fields over the past few decades owing to their solution-based processability,[1] bandgap tunability,[2] and multi-exciton generation properties.[3] For PbS CQDs, they have large Bohr exciton radii (~18 nm),[4] solution processability, tunable bandgaps and a high light conversion quantum yield,[5] which makes them a promising candidate for optoelectronic devices. PbS QD infrared (IR) detectors (up to 1500 nm) have obtained a high detectivity value of 7 × 10^{13} Jones, which is even higher than that of commercial InGaAs photodiodes.[6] Although PbS QD photoconduction detectors are facile to fabricate and demonstrate a high responsivity, they are limited by the response speed, signal to noise ratio and difficulties with the integration of detector arrays. On the contrary, depletion heterojunction based PbS photodiodes can overcome the above limitations and have obtained significant progress in the last few years.[7,8]

The most utilized photodiode device structure is based on the ZnO/PbS CQD heterojunction.[9,10] In order to optimize the ZnO/PbS CQD solar cell performance, it is not necessary to ensure that dark currents will be compellingly low for light harvesting. While in photodetectors (PDs), it is imperative to investigate material strategies that systematically minimize dark current and improve light current due to the high dependence of $D^* \propto J_{\text{dark}}^{-1/2}$, where D^* is the specific detectivity. The total dark current density, J_{dark}, includes both the reverse saturation current density (J_0) of the photodiode and also any parallel shunt path currents. Thus, the interface and bulk defect passivation (IP and BP) played vital roles to suppress dark current so as to improve detector performances. For a ZnO buffer layer, the existence of band tail states seriously increased the J_0 value. An interlayer intercalation which could suppress the recombination of band tail states has been demonstrated as an efficient strategy to minimize J_0.[11] On the other hand, the ultra-high surface area of QD films has motivated the development of a series of ligands for QD surface passivation.[12,13] Iodide salts that featured atomic spacings and an efficient passivation were widely applied in high performance PbS QD optoelectronic devices.[14] In order to not introduce an exotic counterion, lead iodide was utilized for ligand exchange.[15] Simultaneously, it also shows great potential as an intercalation layer due to its high resistivity and compatibility for device fabrication. Thus, the present work investigated the utilization of PbI_2 for both interface and QD surface passivation for high performance PbS QD infrared photodetectors.

Herein, three types of PDs with ZnO/PbS–TBAI (tetrabutylammonium)/PbS–EDT (1,2-ethanedithiol) (the control device), ZnO/PbI_2/PbS–TBAI/PbS–EDT (the IP device) and ZnO/PbI_2/

---

[a] Wuhan National Laboratory for Optoelectronics (WNLO), Huazhong University of Science and Technology (HUST), 1037 Luoyu Road, Wuhan, Hubei, 430074, China. E-mail: songhs-wnlo@mail.hust.edu.cn

[b] Physics Laboratory, Industrial Training Center, Shenzhen Polytechnic, Shenzhen, People's Republic of China. E-mail: caoyulin@szpt.edu.cn

† Electronic supplementary information (ESI) available. See DOI: 10.1039/c7ra10422g

PbS–PbI$_2$/PbS–EDT (the IP/BP device) device structures were designed and implemented by the PbI$_2$ passivation strategy. A series of prototype devices verified a sufficient interface and bulk defect passivation effect with a normalized detectivity of about 10^{13} Jones and an improved efficiency of 8% has been achieved. The combination of the interface and bulk passivation efficiently suppressed the dark current and pronouncedly enhanced the responsivity and detectivity. The presented IP/BP PDs with a convenient operation and an efficiency improvement are expected to make contributions to high performance PbS CQD optoelectronic devices.

Results and discussion

The as-synthesized PbS QDs showed an exciton absorption peak located at 888 nm, shown in Fig. 1a (black curve). Also, the size of the PbS QDs was estimated to be ~2.9 nm according to the Moreels equation and their bandgap was ~1.4 eV.[16] The peak to valley ratio was ~2.88 demonstrating a uniform QD size distribution. In addition, the absorption of the PbI$_2$–DMF solution in Fig. 1a (blue curve) demonstrated an ultra-low response at long wavelengths (>550 nm) with a bandgap of ~2.3 eV. The PbS QD film was further characterized by XRD as shown in Fig. 1b, and the typical diffraction peaks agreed well with those of the PbS standard PDF card (JCPDS no: 02-0699). The broadening and low intensity of the diffraction peaks confirmed the small size of the QDs. Utilizing a photodiode device structure, the obtained PbS QDs were fabricated into heterojunction photodetectors, as shown in Fig. 1c. Comparing with a typical PbS QD photodiode device, ITO/ZnO/PbS–TBAI/PbS–EDT/Au (the control device), the newly developed device has a PbI$_2$ interlayer with a structure of ITO/ZnO/PbI$_2$/PbS–TBAI/PbS–EDT/Au that was denoted as the interfacial passivation (IP) device. Utilizing the energy levels of ITO,[17] ZnO,[9,18] PbI$_2$,[19] PbS–TBAI/PbS–EDT[20] and Au,[21] their energy band alignment diagram was plotted in Fig. 1d. The conduction band minimum of PbI$_2$ is much higher than those of the ZnO and PbS active layer, thus it could introduce a transfer barrier for photocarriers so as to suppress the photodetector dark current.

Photodetector performances are typically evaluated from the responsivity (R), response speed and detectivity (D^*). The responsivity shows the device sensitivity toward light detection and can be calculated from $R = \frac{I_p}{P}$. And, the shot noise derived normalized detectivity can be obtained by $D^* = \frac{I_p\sqrt{A}}{P\sqrt{2qI_d}}$, where I_p is the photocurrent, I_d is the dark current, P denotes the light power density illuminated on the device, A is the device area, and q represents the elementary charge. According to the R and D^* formulas, I_p and I_d contain a trade-off dependence from the insulative PbI$_2$ layer intercalation. Thus, the thickness of the PbI$_2$ layer should be optimized in order to control the I_d and I_p values. A series of PbI$_2$ concentrations from 0 g mL^{-1} to 0.5 g mL^{-1} were investigated and their I–t responses are shown in Fig. 2a, and the photocurrents firstly increased from 15.5 μA to 20.5 μA and then decreased at high PbI$_2$ concentrations. Meanwhile for the dark current values, the IP devices obtained a monotonic decrease indicating an efficient dark current suppression by the insulative PbI$_2$ layer (Fig. 2b). At low concentrations such as 0.05 and 0.0025 g mL^{-1}, the low electron injection barrier had little effect on the photocurrent suppression and simultaneously the thin PbI$_2$ layer could help to passivate the interface defects of ZnO. Thus, the obtained photocurrent was improved similar to the PbI$_2$ passivation

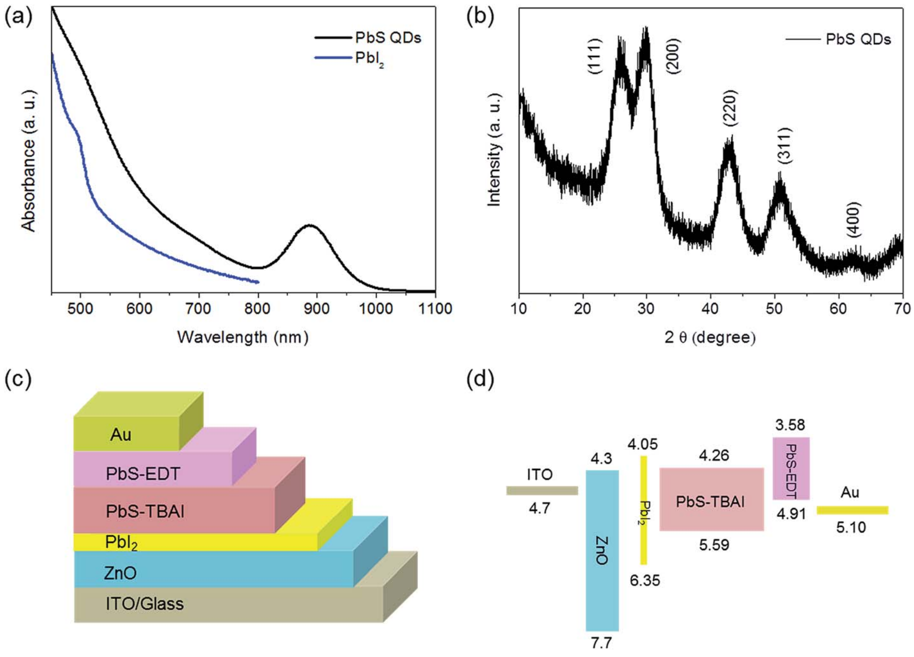

Fig. 1 (a) Absorption spectra of the PbS QDs and PbI$_2$ film. (b) XRD spectrum of the as-synthesized PbS QDs. (c) Schematic device structure diagram of the IP-PDs. (d) Energy band alignment diagram of the IP-PDs.

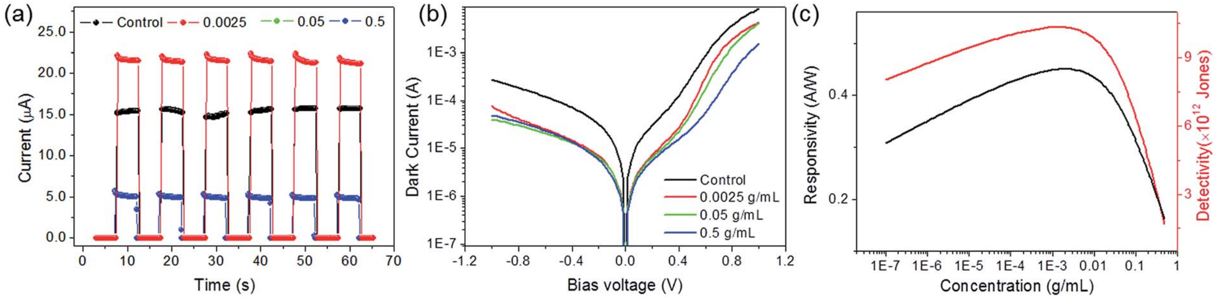

Fig. 2 The performances of the IP-PDs at different PbI_2 concentrations: (a) I–t responses of the IP-PDs. (b) I–V curves in dark conditions under ambient environment with a sweep voltage from −1 V to 1 V. (c) Responsivity (black) and detectivity (red) evolution curves. All the measurements were performed utilizing an 850 nm LED lamp with a 430 μW cm^{-2} light intensity.

effect in perovskite photodetectors.[22] If the PbI_2 concentration was further increased (~0.5 g mL^{-1}), the injection barrier was elevated and led to a decrease of the photocurrent. As a consequence, the optimized concentration was 0.0025 g mL^{-1} which could implement the trade-off between the I_p improvement and I_d suppression. Similarly, the responsivity and detectivity showed the same evolution trend as the PbI_2 concentrations varied and obtained a peak value of 0.57 A W^{-1} and 9.54×10^{12} Jones, respectively (Fig. 2c). Also, the R and D^* values of the control devices were 0.43 A W^{-1} and 5.23×10^{12} Jones, respectively. Therefore, the accession of the PbI_2 interlayer PDs carried out the suppression of I_d and the enhancement of I_p compared with the control device.

As well as interface passivation, ultra-high surface area QD absorbers should be efficiently capped by short chain ligands for enhancing the photocarrier transport and surface dangling bond passivation.[15] PbI_2 could be utilized not only for interface passivation but also as an efficient QD ligand for the passivation of absorber bulk defects by a phase-transfer ligand exchange process.[23] Thus, the integration of both the interface and bulk passivation photovoltaic PDs could be facilely implemented utilizing PbI_2.

The PbI_2 phase-transfer ligand exchange process is roughly described in the inset of Fig. 3a. The starting materials were PbS QD octane solution and PbI_2–DMF solution. When the black PbS–OA QD octane solution was added into the yellow PbI_2–DMF solution with an equal volume, an obvious delamination was obtained owing to the immiscible property between octane and DMF (left). After 15–30 minutes of vigorous stirring for ligand exchange, the black PbS QDs transferred to the bottom DMF solution. Also, the QD ligand was exchanged from OA to PbI_2 with transparent octane left. The corresponding exciton absorption peak shifted from 878 nm to 919 nm. The detailed comparative characterizations before and after the PbI_2 treatment are shown in Fig. S1–S3 (ESI†). Therefore, the phase-transfer ligand exchange process could be facilely implemented in one step demonstrating a more convenient and efficient operation than the traditional layer-by-layer (LBL) method. The Fourier transform infrared (FTIR) spectrum of the PbI_2 treated film (red line) in Fig. 3b has nearly no characteristic peaks of the OA ligand (*i.e.*, C–H, C=O). Thus, the phase-transfer ligand exchange process can sufficiently remove the surface OA ligand.

Utilizing the strategies of IP and BP, photovoltaic PDs were fabricated to investigate the PbI_2 passivation effect. The schematic diagram of the IP/BP PD device is shown in Fig. 4a with a structure of ITO/ZnO/PbI_2/PbS–PbI_2/PbS–EDT/Au, where the PbI_2 material not only acted as the interface passivation layer but also worked as the QD absorber ligand. The photoresponse for the IP and IP/BP devices is shown in Fig. 4b. The photocurrent of the IP/BP devices further increased from 19 μA to 21 μA, which manifested the improved QD surface passivation by

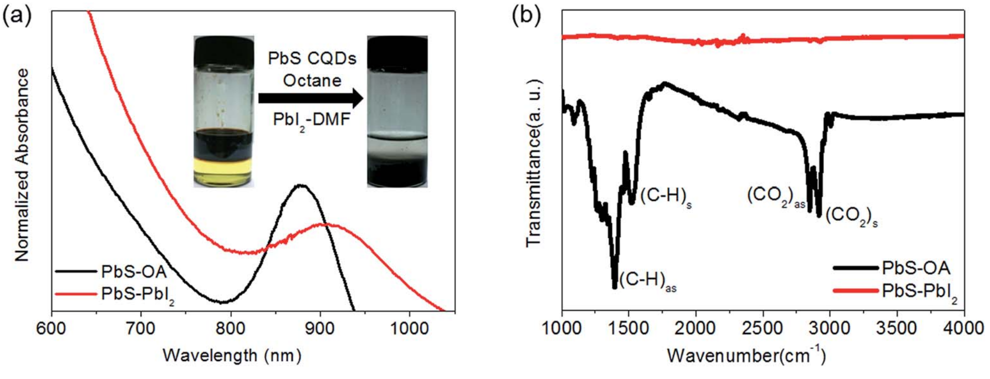

Fig. 3 (a) Absorption spectra of the PbS QDs before (black) and after the PbI_2 treatment (red). The inset shows the solution-processed phase transfer process. (b) FTIR spectra of PbS–OA and PbS–PbI_2.

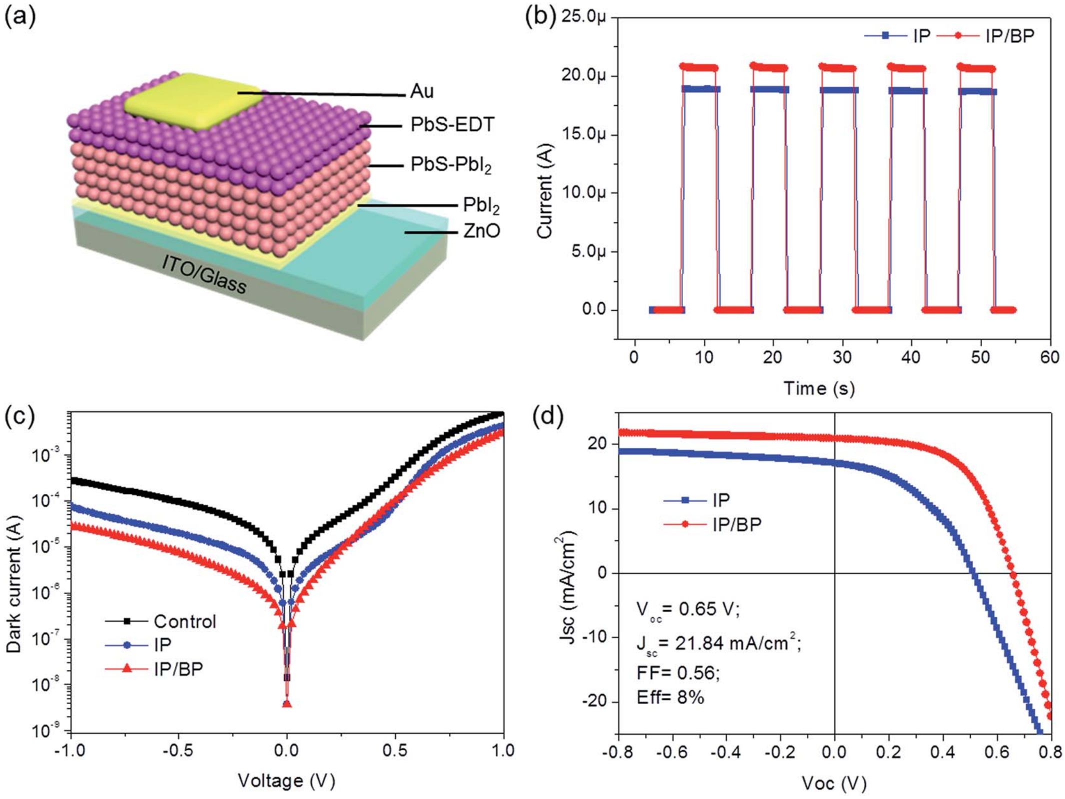

Fig. 4 Comparative analysis between the IP-PDs and IP/BP-PDs. (a) A schematic device structure diagram of the IP/BP photovoltaic PDs. (b) I–t curves of the IP and IP/BP PDs. The measurements were performed utilizing an 850 nm LED lamp with a 430 μW cm^{-2} light intensity at 0 V bias. (c) Dark I–V curves of the control and the IP and IP/BP PDs under ambient environment with a sweep voltage from −1 V to 1 V. (d) J–V curves of the IP and IP/BP based devices tested under 100 mW cm^{-2} AM 1.5G illumination.

the PbI_2 ligands compared with the traditional TBAI one. Furthermore, the low dark currents are drawn in a logarithmic plot, the dark current could be gradually decreased from the control PDs (2.82 × 10^{-4} A, black curve) to the IP/BP PDs (2.85 × 10^{-5} A, red curve) (Fig. 4c), which is one order of magnitude lower than that of the control one. On the other hand, the IP/BP photovoltaic PDs could also be applied in energy conversion and their current density–voltage (J–V) curves are shown in Fig. 4d. The IP/BP devices obtained an efficiency of 8% ($V_{oc} = 0.65$ V, $J_{sc} = 21.84$ mA cm^{-2} and FF = 0.56), which is almost double the value of the IP devices (4.2%).

The two most important figures of merit for the photodetector, the responsivity and detectivity, were also measured to evaluate the PD performances, as shown in Fig. 5. As the applied bias was increased, their responsivity monotonically increased. The R values of the IP/BP PDs slightly increased from 0.42 A W^{-1} to 0.53 A W^{-1} as the reverse bias increased from 0 V to −1 V. Meanwhile, the control device obtained lower values which evolved from 0.21 A W^{-1} to 0.31 A W^{-1} as the bias was varied. The small bias-dependent R values manifested the depletion of the heterojunction and transfer barrier effect from PbI_2. At the same applied bias, the IP/BP devices obtained higher R values indicating a passivation effect from the IP and BP treatment. For the bias dependence of the specific detectivity (Fig. 5b), it scaled with $J_d^{-1/2}$, thus it obtained a peak value of 4.91 × 10^{12} Jones at low bias. This was one order higher than that of the control device and comparable to those of commercial silicon photodetectors in the IR spectrum.[24] To study the device response under a varied input irradiance, the control and IP/BP PDs were excited by a wider-bandgap laser at $\lambda = 650$ nm. The responsivity and detectivity of the measured devices were linear across a wide range from 10^{-6} W cm^{-2} to 10^{-3} W cm^{-2} with high quantum yields (Fig. 5c and d). A high D* value of 1.3 × 10^{13} Jones was obtained from the IP/BP PDs at 0 V bias.

Normalized photocurrent–time curves are shown in Fig. 6a. Under the same measurement conditions, the IP/BP devices obtained 5.3 μs for the rise time and 4.9 μs for the decay time, respectively, which were also better than the corresponding values of the control devices (10 μs and 7 μs). The faster response time of the IP/BP devices further demonstrated an efficient interface and bulk defect passivation. The linear dynamic range (LDR) or photosensitivity linearity and 3 dB bandwidth are key parameters for characterizing the detectable linear light intensity of QD PDs. According to the equation reported in the literature LDR = 20 log(J_{ph}/J_d),[25] where J_{ph} is the photocurrent measured at a light intensity of 1 mW cm^{-2}. The LDR values of the IP/BP and control devices were calculated to be 101.28 dB and 92.78 dB, respectively (Fig. 6b), which were close to that of Si PDs (120 dB) and much higher than that of InGaAs PDs (66 dB).[26] The 3 dB bandwidth of the IP/BP device

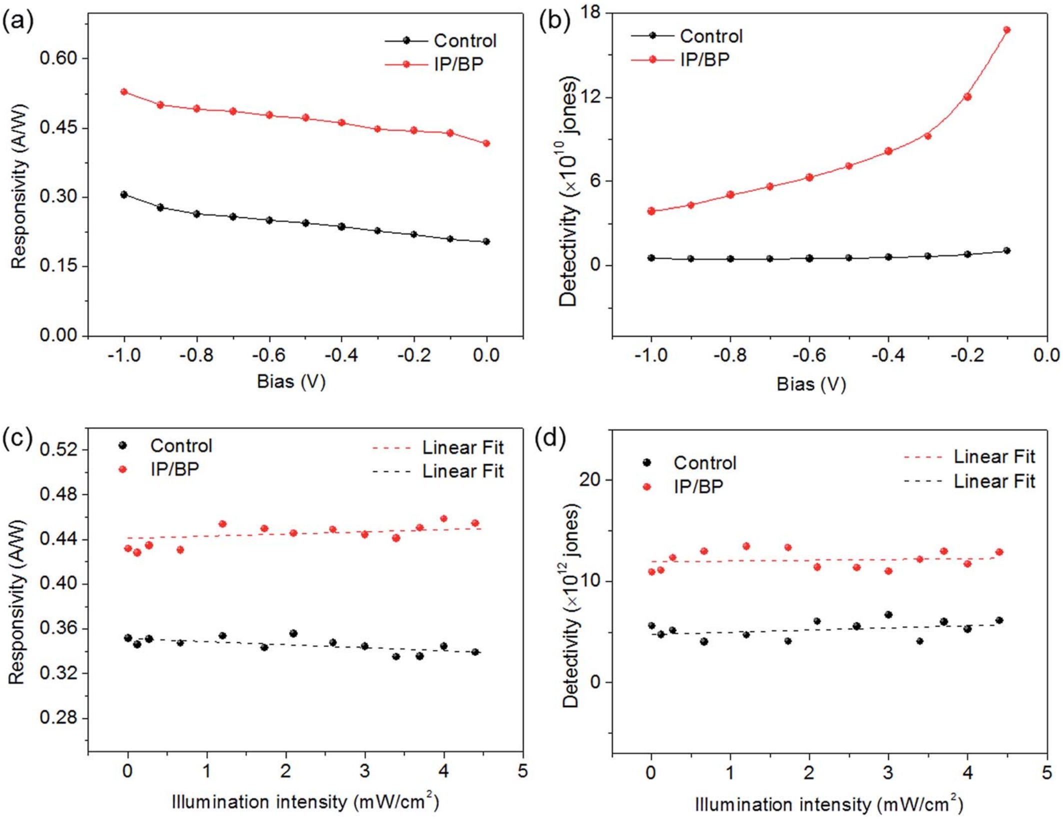

Fig. 5 (a and b) Bias dependence of the responsivity and detectivity. The measurements were performed utilizing an 850 nm LED lamp with a 430 μW cm^{-2} light intensity. (c and d) The responsivity and detectivity dependence on the incident illumination intensity. The measurements were performed utilizing a 650 nm LED lamp with a 430 μW cm^{-2} light intensity at 0 V bias.

could reach 5 kHz (Fig. 6c), which is much higher than that of the control device (1 kHz) verifying the fast response of the IP/BP device.

According to the above comparison analysis, a pronounced enhancement was obtained from the IP/BP devices. A possible mechanism for the improvement is schematically described in Fig. 7. For the control device utilizing TBAI as the ligand, there may exist sub-bandgap defect states for the absorber layer and interface defects originating from oxidation species in the PbS QDs–TBAI film (Fig. 7a).[27] In contrast, the sub-bandgap states can be removed and favor carrier transfer by the PbI_2 treatment for the interface and QD ligands (Fig. 7b). Meanwhile, the conduction band of a thin layer of PbI_2 was a little higher than those of ZnO and PbS–TBAI, so it could work as a barrier for electron injection and thus suppressed the dark current. Therefore, the IP/BP devices could reduce the bulk recombination and enhance the charge carrier collection efficiency for the photovoltaic PDs.

The normalized transient photovoltage decay is shown in Fig. 7c. The decay time of the IP/BP device (590 μs) is much slower

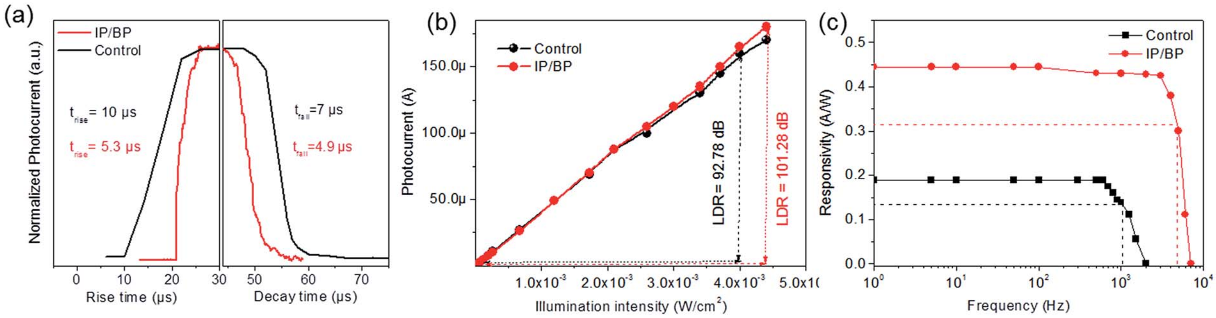

Fig. 6 Performances of the control device and IP/BP-PDs. (a) The normalized photocurrent decay of the control and IP/BP devices. (b) Photocurrent linearity upon the incident light intensity. (c) Responsivity evolution with the input signal frequency. All the measurements were performed utilizing an 850 nm LED lamp with a 430 μW cm^{-2} light intensity at 0 V bias.

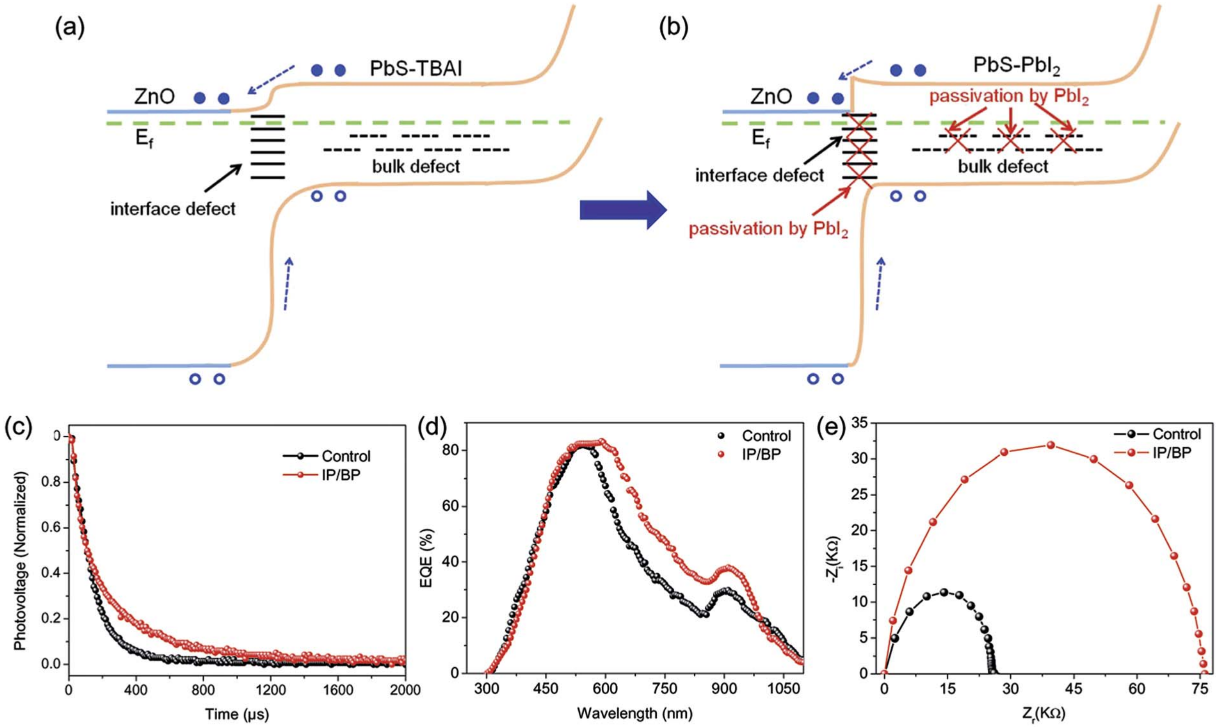

Fig. 7 (a) Schematic energy–band diagram for TBAI treated PbS QD PDs. (b) Energy–band diagram of the IP/BP treated PDs. (c) The normalized photovoltage decay of the control and IP/BP devices. (d) EQE spectra of the control and IP/BP PDs. (e) EIS diagrams of the IP/BP PDs and control device.

than that of the control one (282 μs). It can be inferred that the charge recombination lifetime of the IP/BP devices is much longer than that of the control device, and thus could improve PD performances. An external quantum efficiency (EQE) was measured in order to further verify the spectra dependent quantum yields. Both the IP/BP and control devices demonstrated wide spectra and a high EQE response (Fig. 7d). In the spectra at high photon energies (300–560 nm), the EQE values of the IP/BP device were nearly the same as those of the control device. At longer wavelengths (570–980 nm), the EQE values of the IP/BP devices were much higher than those of the control one. As the EQE values in the spectra at long wavelengths highly depended on the bulk passivation and carrier transport, this further verified the IP and BP treatment functions. Therefore, the IP/BP devices could obtain a higher photocurrent up to 21.84 mA cm^{-2}, in good agreement with the measured J_{sc}. Electrochemical impedance spectroscopy (EIS) is a powerful tool to understand photocarrier transport related information. Fig. 7e shows the EIS spectra of the control and IP/BP devices and that the IP/BP devices obtained a smaller series resistance and larger shunt resistance compared with the control device. The enhanced performance of the IP/BP PDs is similar to the prediction results, which verified the superior effect of the combination of interface and bulk passivation.

In order to make clear whether the PD signal was from thermal effects or light conversion, the temperature dependent responsivity of the PbI$_2$ treated PbS QDs was investigated from 80–300 K (Fig. S4†). The responsivity contained little increase (<5%), which may be ascribed to a temperature increase. However, the main contribution of the obtained photodetector signal was achieved from light conversion rather than a temperature increase. Thus, the present PD detection was stable avoiding the effect of temperature change within the above measurement range.

Conclusions

In summary, we have systematically demonstrated IP/BP PDs by utilizing PbI$_2$ for the interface passivation and QD ligand. A series of PDs were fabricated and demonstrated passivation capability. The PbI$_2$ layer intercalation could elevate the photocurrent and reduce the dark current at the same time by interface-passivation and a carrier-transferring-barrier effect. The developed IP/BP PDs combining interface and bulk passivation together have successfully increased the photocurrent to 4 times higher and suppressed the dark current to one-tenth lower than those of the control device. It's worth mentioning that a high detectivity (1.3 × 10^{13} Jones) and efficiency (8%) were also obtained in the IP/BP PDs. The efficient passivation potential and convenient operation process of the present IP/BP PDs could shed light on the further study of advanced PbS QD optoelectronic devices.

Experimental section

PbS CQD and QD ink synthesis

The QDs were synthesized according to the method of Hines[28] with slight modifications.[29] The PbI$_2$ ligand passivated PbS CQD ink was prepared according to the literature method.[23]

ZnO film fabrication

The ZnO precursor solution was obtained by dissolving 1.5 g of zinc acetate dehydrate (99%) in 20 mL of 2-methoxyethanol (99%) with 0.4 mL of ethanolamine (99%) at 60 °C for 10 h under vigorous stirring. The ZnO film was prepared by spin-coating the precursor on a clean ITO substrate at 4000 rpm for 30 s and then annealing at 400 °C for 15 min. The above step was repeated for several times to reach the desired thickness.

Device fabrication

For the layer-by-layer (LBL) method, the PbS QD film was deposited by spin-coating the QD octane solution on the ZnO coated ITO substrate with or w/o the PbI_2 (in DMF, *ca.* 0.5, 0.05, and 0.0025 g mL^{-1}) interface layer at 2500 rpm for 30 s. The ligand exchange was conducted by dropping 10 mg mL^{-1} tetrabutylammonium (TBAI) (in methanol) and then spinning with the same speed once and rinsing twice with methanol to remove the residual TBAI. Such a deposition process was repeated for 8–10 times to get the desired thickness. For a one step method, the QD film was made by spin-coating at 400–600 rpm and then annealing at 90 °C for 1 min. Subsequently, two layers of EDT treated QDs were deposited through spin-coating the PbS QD octane solution at the same speed followed by one time EDT acetonitrile (0.01%) treatment and acetonitrile washing 2 times. Finally, Au electrodes (~100 nm thick) were made with a shadow mask (0.09 cm^2) by thermal evaporation.

Characterization and measurements

The materials were characterized by UV-Vis absorption spectroscopy (Cary, Lambda 950) and X-ray diffraction spectrsocopy (XRD, XRD-7000S/L). Performances of the PDs were measured using a probe station connected to an Agilent B1500A semiconductor characterization system. Illumination was generated from different light-emitting diodes with different absorption peaks controlled by a functional generator (Agilent 33210A). The light intensity was calibrated using a silicon PD (Newport 818-UV). The *J–V* curves were measured using a Keithley 2400 source unit with a xenon lamp (Newport, 3A solar simulator, 94023A-U, Germany) as simulated AM 1.5G irradiation at 100 mW cm^{-2} under ambient air conditions. The EQE spectra were taken using a home-made setup containing a Keithley 2400 source measure unit and Newport monochromator. The output power was also calibrated by a Si photodiode. EIS was performed on an electrochemical workstation (ZAHNER Zennium, Germany) in the dark state with the frequency ranging from 10 μHz to 4 MHz.

Conflicts of interest

There are no conflicts to declare.

Acknowledgements

This work was financially supported by the Foundation of the Shenzhen Science and Technology Innovation Committee (JCYJ20170413113645633), the Major State Basic Research Development Program of China (2016YFB0700702), the National Natural Science Foundation of Hubei Province (2016CFB431), and the Fundamental Research Funds for the Central Universities (HUST:2016YXMS032). YLC thanks the financial support from the Youth Innovation Foundation of Shenzhen Polytechnic (601722K35019). The authors also thank the Testing Centre of HUST and the Center for Nanoscale Characterization and Devices, Wuhan National Laboratory for Optoelectronics (WNLO), for facility access.

References

1 S. A. McDonald, G. Konstantatos, S. Zhang, P. W. Cyr, E. J. D. Klem, L. Levina and E. H. Sargent, *Nat. Mater.*, 2005, **4**, 138–142.
2 Q. H. Li, X. Jin, Y. Yang, H. N. Wang, H. J. Xu, Y. Y. Cheng, T. H. Wei, Y. C. Qin, X. B. Luo, W. F. Sun and S. L. Luo, *Adv. Funct. Mater.*, 2016, **26**, 254–266.
3 V. Sukhovatkin, S. Hinds, L. Brzozowski and E. H. Sargent, *Science*, 2009, **324**, 1542–1544.
4 W. L. Ma, J. M. Luther, H. M. Zheng, Y. Wu and A. P. Alivisatos, *Nano Lett.*, 2009, **9**, 1699–1703.
5 J. P. Clifford, G. Konstantatos, K. W. Johnston, S. Hoogland, L. Levina and E. H. Sargent, *Nat. Nanotechnol.*, 2009, **4**, 40–44.
6 J. W. Lee, D. Y. Kim and F. So, *Adv. Funct. Mater.*, 2015, **25**, 1233–1238.
7 X. Dai, Z. Zhang, Y. Jin, Y. Niu, H. Cao, X. Liang, L. Chen, J. Wang and X. Peng, *Nature*, 2014, **515**, 96–99.
8 X. W. Gong, Z. Y. Yang, G. Walters, R. Comin, Z. J. Ning, E. Beauregard, V. Adinolfi, O. Voznyy and E. H. Sargent, *Nat. Photonics*, 2016, **10**, 253–257.
9 P. H. Rekemeyer, S. Chang, C.-H. M. Chuang, G. W. Hwang, M. G. Bawendi and S. Gradečak, *Adv. Energy Mater.*, 2016, **6**, 1600848.
10 Z. Yang, A. Janmohamed, X. Lan, F. P. Garcia de Arquer, O. Voznyy, E. Yassitepe, G. H. Kim, Z. Ning, X. Gong, R. Comin and E. H. Sargent, *Nano Lett.*, 2015, **15**, 7539–7543.
11 X. L. Zhang and E. M. J. Johansson, *J. Mater. Chem. A*, 2017, **5**, 303–310.
12 J. B. Zhang, J. B. Gao, E. M. Miller, J. M. Luther and M. C. Beard, *ACS Nano*, 2014, **8**, 614–622.
13 J. Tang, L. Brzozowski, D. A. Barkhouse, X. Wang, R. Debnath, R. Wolowiec, E. Palmiano, L. Levina, A. G. Pattantyus-Abraham, D. Jamakosmanovic and E. H. Sargent, *ACS Nano*, 2010, **4**, 869–878.
14 J. Tang, K. W. Kemp, S. Hoogland, K. S. Jeong, H. Liu, L. Levina, M. Furukawa, X. Wang, R. Debnath, D. Cha, K. W. Chou, A. Fischer, A. Amassian, J. B. Asbury and E. H. Sargent, *Nat. Mater.*, 2011, **10**, 765–771.
15 D. N. Dirin, S. Dreyfuss, M. I. Bodnarchuk, G. Nedelcu, P. Papagiorgis, G. Itskos and M. V. Kovalenko, *J. Am. Chem. Soc.*, 2014, **136**, 6550–6553.
16 I. Moreels, K. Lambert, D. Smeets, D. De Muynck, T. Nollet, J. C. Martins, F. Vanhaecke, A. Vantomme, C. Delerue, G. Allan and Z. Hens, *ACS Nano*, 2009, **3**, 3023–3030.

17 J. R. Manders, T.-H. Lai, Y. B. An, W. K. Xu, J. Lee, D. Y. Kim, G. Bosman and F. So, *Adv. Funct. Mater.*, 2014, **24**, 7205–7210.

18 H. P. Lu, J. Joy, R. L. Gaspar, S. E. Bradforth and R. L. Brutchey, *Chem. Mater.*, 2016, **28**, 1897–1906.

19 J. X. Song, E. Q. Zheng, J. Bian, X. F. Wang, W. J. Tian, Y. Sanehira and T. Miyasaka, *J. Mater. Chem. A*, 2015, **3**, 10837–10844.

20 C. H. M. Chuang, P. R. Brown, V. Bulovic and M. G. Bawendi, *Nat. Mater.*, 2014, **13**, 796–801.

21 J. Chang, Y. Kuga, I. Mora-Sero, T. Toyoda, Y. Ogomi, S. Hayase, J. Bisquert and Q. Shen, *Nanoscale*, 2015, **7**, 5446–5456.

22 H. L. Zhu, J. Cheng, D. Zhang, C. Liang, C. J. Reckmeier, H. Huang, A. L. Rogach and W. C. Choy, *ACS Nano*, 2016, **10**, 6808–6815.

23 H. Aqoma, M. Al Mubarok, W. T. Hadmojo, E. H. Lee, T. W. Kim, T. K. Ahn, S. H. Oh and S. Y. Jang, *Adv. Mater.*, 2017, **29**, 1605756.

24 Y. Zhang, Y. Yu, L. Mi, H. Wang, Z. Zhu, Q. Wu, Y. Zhang and Y. Jiang, *Small*, 2016, **12**, 1062–1071.

25 X. Gong, M. H. Tong, Y. J. Xia, W. Z. Cai, J. S. Moon, Y. Cao, G. Yu, C.-L. Shieh, B. Nilsson and A. J. Heeger, *Science*, 2009, **325**, 1665–1667.

26 C. Liu, K. Wang, P. Du, E. Wang, X. Gong and A. J. Heeger, *Nanoscale*, 2015, **7**, 16460–16469.

27 C. H. M. Chuang, A. Maurano, R. E. Brandt, G. W. Hwang, J. Jean, T. Buonassisi, V. Bulovic and M. G. Bawendi, *Nano Lett.*, 2015, **15**, 3286–3294.

28 M. A. Hines and G. D. Scholes, *Adv. Mater.*, 2003, **15**, 1844–1849.

29 K. Qiao, H. Deng, X. Yang, D. Dong, M. Li, L. Hu, H. Liu, H. Song and J. Tang, *Nanoscale*, 2016, **8**, 7137–7143.